Three generalizations of the fully frustrated triangular XY model

W.-M. Zhang and W. M. Saslow
Physics Department, Texas A&M University, College Station, Texas 77843

M. Gabay and M. Benakli
Laboratoire de Physique des Solides, Université de Paris-Sud, 91405 Orsay, France

(Received 8 February 1993; revised manuscript received 20 May 1993)

The fully frustrated triangular lattice of XY spins has nearest-neighbor antiferromagnetic interactions and a locally ordered state with three spins per unit cell, at 120° to one another. Using mean-field theory and a fluctuation analysis, we have studied three generalizations, as a function of a parameter η, each of which reduces to the original model for $\eta=1$. The investigation arose from an attempt to obtain, for the fully frustrated triangular lattice of XY spins, the same type of generalization that was obtained by Berge *et al.* for Villain's "odd" model of fully frustrated XY spins on the square lattice. The three generalizations are: the "row" model, which has a preferred direction and one spin per unit cell in its Hamiltonian; the "centered honeycomb" model, which has three spins per unit cell in its Hamiltonian; and the "staggered row" model, which has three spins per unit cell and a preferred direction in its Hamiltonian. The "staggered row" model is the most complex of the three, with aspects of each of the other models and an (η, T) phase diagram possessing five ordered phases and two tetracritical points. Its spiral (with three spins per unit cell) SP3 and its antiferromagnetic (with six spins per unit cell) AF6 phases are much like the spiral SP and antiferromagnetic AF phases of the row model; its ferrimagnetic (FI) and AF3 phases have the same symmetry as the corresponding phases of the "centered honeycomb" model, and its noncollinear NC6 phase is related to the NC3 phase of the "centered honeycomb" model. Comparison between the models enables us to distinguish those properties that are due to three spins per unit cell from those due to the preferred direction. From the phase diagrams, we conclude that the "centered honeycomb" lattice is the sought-after generalization. An analysis of the various transitions in all three models is made, to identify Ising-like and XY-like transitions. For the "staggered row" model, a fluctuation analysis that includes phase fluctuations but not amplitude fluctuations is also performed, yielding insight into the nature of the ordered phases, and the significance of the two tetracritical points. Our analysis of the phase diagram for the "centered honeycomb" model suggests that $RbFeBr_3$ may, at low enough temperatures, undergo a phase transition from a collinear to a canted state.

I. INTRODUCTION

Two-dimensional (2D) XY spin systems have recently been the subject of a review devoted to the possibility of their experimental realization.[1] In some of the theoretical models, competing interactions play an important role. Such interactions lead to frustration[2–4] and make spin systems exhibit rich phase structure and critical phenomena. The present work is devoted to the study of three related models of frustrated XY spin systems on a triangular lattice, with a view to understanding the nature of the phases that appear and the reasons why certain models yield commensurate states and others do not. Our results were largely obtained using mean-field theory and a fluctuation analysis. Because fluctuations in two dimensions are well known to destroy long-range order in continuous valued order parameters such as spin orientation, our interest is restricted to the nature of the *local* order of the phases and of the phase diagrams.

One of the earliest studied models of frustrated XY spins in two dimensions is Villain's "odd" model of fully frustrated XY spins on the square lattice.[2] In this model each plaquette has three ferromagnetic bonds and one antiferromagnetic nearest-neighbor bond of equal strength. Berge *et al.* generalized this model by replacing the antiferromagnetic bonds $-J$ with $-\eta J$,[4] where $\eta=1$ gives the Villain model. Using Monte Carlo simulations, they then obtained a rich $(\eta, T/J)$ phase diagram with a tetracritical point at $\eta=1$, $T/J\approx 0.45$. Reference 5 studied this generalized Villain model by mean-field theory, obtaining a phase diagram similar to that of the Monte Carlo calculations and, because the mean-field theory identified the local order of each state, provided a physical explanation for the divergences in the magnetic susceptibility found in Ref. 4.

For the triangular lattice, there is also a fully frustrated XY model (which we shall refer to as the FFTR model). In this case the model involves only nearest-neighbor antiferromagnetic interactions. The FFTR model has been the subject of much theoretical study.[6–10] One of the more interesting aspects of this model is the nature of the phase diagram when a magnetic field is applied, where a new phase, not anticipated in mean-field theory, appears. (An analog, for the square lattice, which has similar properties, involves up to third-neighbor interactions.[11] We will not discuss this model further.) One of the motivations for the present work was to find analogs for the FFTR model of the generalization of Berge *et al.* for

the fully frustrated XY model on the square lattice.

A number of real systems are related to the FFTR model. For example, a large class of insulators with the chemical formula ABX_3 crystallize into a hexagonal lattice.[12,13] The nearest-neighbor interactions, due to superexchange, are antiferromagnetic. Moreover, the dipolar interactions tend to restrict the magnetic moments to the ab plane. Thus, within the ab plane there is a tendency to form the 120° structure characteristic of the ground state of the FFTR model,[6–8] and the strong antiferromagnetic interplanar interaction causes this order to be propagated along the c axis with planes of alternating chirality. One example is $CsMnBr_3$, which has been studied in Ref. 12. This work shows that at low temperatures the nearest-neighbor Mn spins indeed are rotated by 120° with respect to one another, consistent with the ground state of the FFTR model. Kawamura and others have argued that materials with this structure have critical exponents that are characterized by a new universality class.[14–16]

In another material, $RbMnBr_3$, a helical spin ordering with $T_N \approx 8.8$ K is found that is incommensurate with the underlying triangular lattice.[13] It has been argued that this is due to a uniform distortion of the lattice[17] that retains one spin per unit cell, but leads to exchange bonds described by what we call the "row" model.[18] The 130° turn angle corresponds to $\eta = 0.78$ in the row model.

Another type of structure is found in the system $RbFeBr_3$. The dominant interactions in this system are antiferromagnetic along the normal to the triangular planes. In addition, at low temperatures it undergoes a structural deformation (one-third of the atoms corresponding to the triangular lattice leave the triangular plane), giving it a lattice symmetry that, in the plane, corresponds to what we shall call the "centered honeycomb" model.[17,19,20] We will see that this model, with three spins per unit cell, has a phase diagram in η-T space that is most closely analogous, for the FFTR model, of the generalization of Berge *et al.* for the fully frustrated XY model on the square lattice. Note that the symmetry found experimentally is compatible with either of two ordered states, and that the present work suggests that, at lower temperatures, the $RbFeBr_3$ system may undergo a phase transition from a collinear to a canted state. Because of the strong antiferromagnetic interactions between the planes, no diverging magnetic susceptibility at the transition and no net moment in the ordered state would be observed.

In addition to these models, a third model which we call the "staggered row" model, has been introduced and studied.[21] Like the centered honeycomb model, it has three spins per unit cell, but it also has a preferred direction, one consequence of which is the possibility of spiral states. Presently it appears to have no known experimental realizations, but it has properties that are related to honeycomb model.

We now present the three models in more detail.

A. Row model

For the row model,[17,18] all the horizontal bonds possess a bond strength of $-\eta J$ instead of $-J$. The spin Hamiltonian, nevertheless, still has only one spin per unit cell. There are two ordered phases. For $\eta > 0.5$, the system goes into a spiral phase SP with one spin per unit cell, which for $\eta = 1$ is commensurate with the periodicity of the lattice. See Fig. 1(a), which also defines the bonds in the system. For $\eta < 0.5$, the system goes into an antiferromagnetic state AF with ferromagnetic rows whose direction alternates as one moves vertically [see inset in Fig. 1(b)]. The $(\eta, T/J)$ phase diagram, including the thermally disordered state P, is given in Fig. 1(b). Using the "spiraling" algorithm, a collective Monte Carlo step that was developed specifically to let the system choose its own boundary conditions, this system has been studied using the Monte Carlo method.[22] The Monte Carlo phase diagram is qualitatively similar to the mean-field phase diagram.

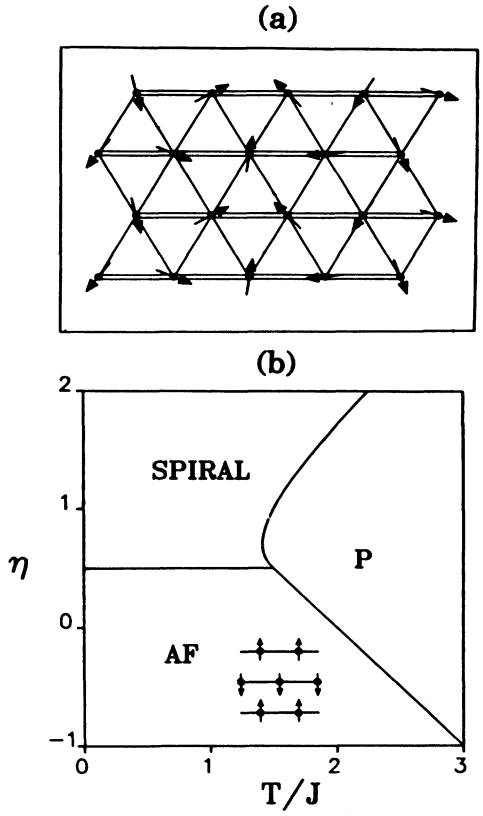

FIG. 1. (a) Exchange bonds for the row model (the single bonds are $-J$; the double bonds are $-\eta J$) and the spiral phase for $\eta = 2$; (b) phase diagram for the row model, with the AF phase defined in inset.

B. Staggered row model: Commensurate and three-spins-per-cell solution

For the "staggered row" model, only every third horizontal bond is changed to a strength $-\eta J$ instead of $-J$, thus leading to a Hamiltonian with three spins (A,B,C) per unit cell. See Fig. 2. Assuming that the only relevant states have three spins per cell, Parker, Saslow, and Ga-

bay obtained the mean-field phase diagram for this system.[21] For zero external field, the $(\eta, T/J)$ phase diagram of Ref. 21, given in Fig. 3, is very similar to that of Ref. 5. In the AF3 state of Fig. 2(a) (the 3 because there are three spins per unit cell, to distinguish it from the AF state of the row model, which has two spins per unit cell), spins A and B are opposed and spin C "melts." (The AF3 state was called the AF state in Ref. 21.) In the ferrimagnetic (FI) state of Fig. 2(b), spins A and B are opposite to C, and the system has a net magnetization. There is also a noncollinear state NC3, shown in Fig. 2(c),

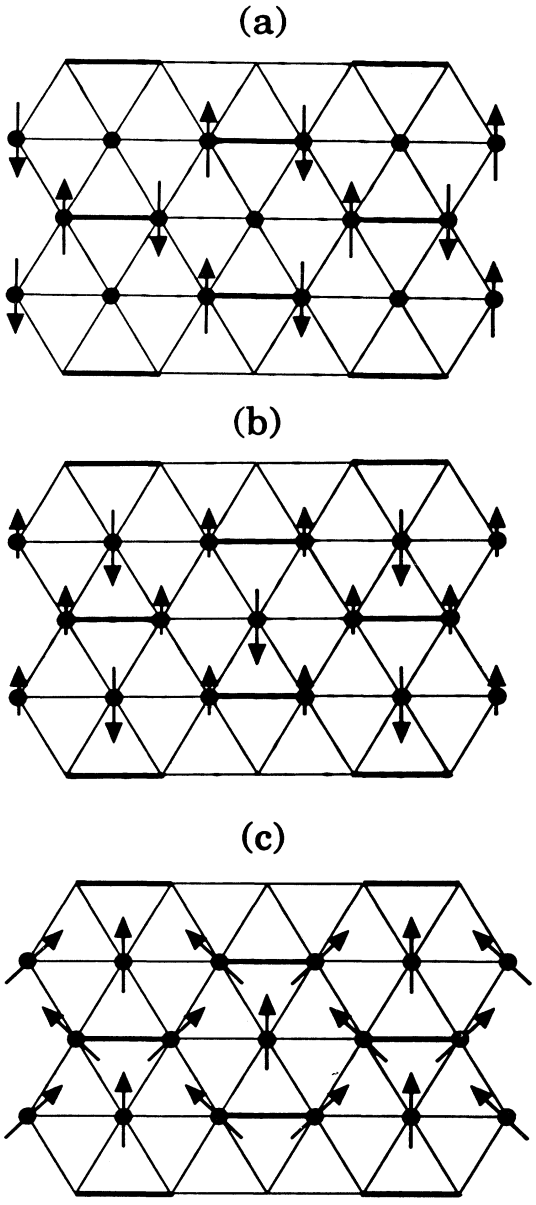

FIG. 2. Various phases obtained for the staggered row model, assuming that the solutions are commensurate with three spins per unit cell. The exchange bonds are drawn on each of these phases: (a) AF3 phase, (b) FI phase, (c) NC3 phase. The light bonds are $-J$; the dark bonds are $-\eta J$.

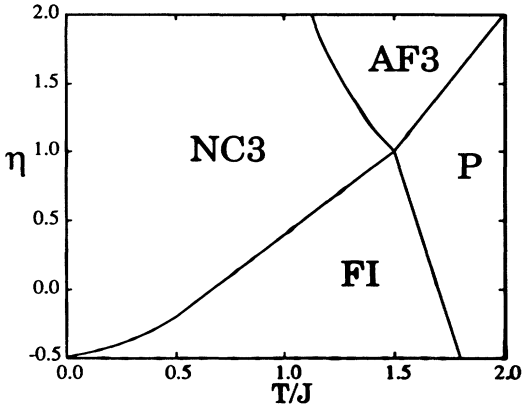

FIG. 3. Phase diagram for the staggered row model, assuming that the solutions are commensurate with three spins per unit cell. The states are defined in Fig. 2.

which is not a minimum on expanding the space of solutions to include incommensurate and six-spin–cell solutions. (The NC3 state was called the NC state in Ref. 21.) It was originally thought that the staggered row model was the sought-after analog for the FFTR model of the generalization of Berge *et al.* for the fully frustrated XY model on the square lattice, because of the similarity of its η-T phase diagram[21] to those of Refs. 4 and 5. As will be seen below, the actual phase diagram is not that of Fig. 3, so that the staggered row model is not the desired generalization.

C. Centered honeycomb model

For the centered honeycomb model, all the bonds along the honeycomb are $-\eta J$, and all the bonds from the centers of the honeycombs are $-J$. The spin Hamiltonian has three spins per unit cell. See Fig. 4. The mean-field theory for this system, assuming commensurate solutions with three spins per unit cell, is analyzed in Sec. VI, where it is shown to be closely related to the mean-field theory of the commensurate three-spins-per-unit-cell solution for the staggered row model. Thus the NC3, AF3, and FI states of Fig. 2 occur, although the exchange bonds are different. The $(\eta, T/J)$ phase diagram for the centered honeycomb model is given in Fig. 5.

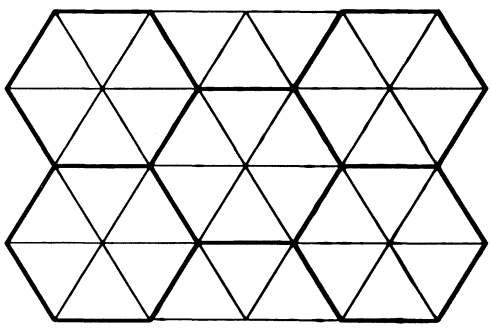

FIG. 4. Exchange bonds for the centered honeycomb model. The light bonds are $-J$; the dark bonds are $-\eta J$.

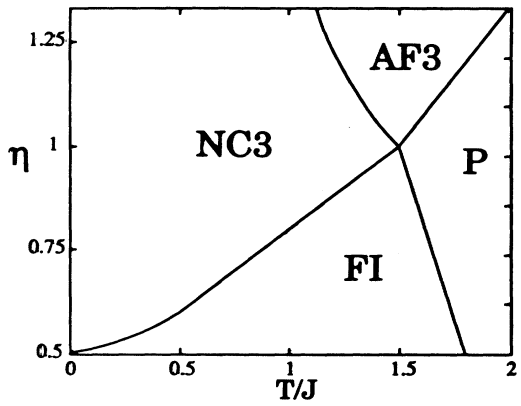

FIG. 5. Phase diagram for centered honeycomb model. The states are defined in Fig. 2.

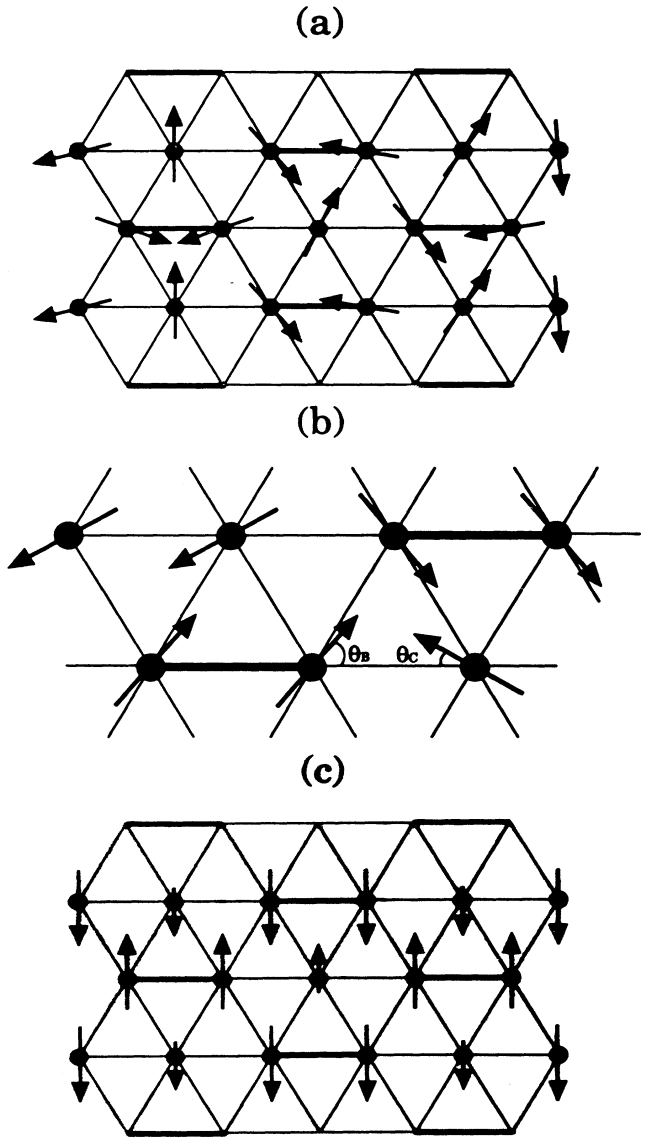

FIG. 6. New phases occurring for the staggered row model when incommensurate and six-spins-per-unit-cell solutions are included: (a) SP3, (b) NC6, (c) AF6.

Comparison of Fig. 5 to the phase diagrams given in Refs. 4 and 5 reveals a great similarity and enables us to conclude that the centered honeycomb model is the desired generalization. Note that Ref. 17, which considered only $T=0$, also obtained the NC3 phase. Reference 19 is consistent with either the NC3 or AF3 phase. However, since the phase diagram of Fig. 5 indicates that, for $\eta > 1$ on cooling, the collinear AF3 phase will be attained first, it suggests that, on further cooling, the system may undergo a phase transition to the canted NC3 state. Note that, because of the strong antiferromagnetic interaction between planes, there will be no divergence in the magnetic susceptibility at the transition, and no net magnetic moment in the canted state.

D. Staggered row model: Incommensurate and six-spins-per-cell solution

Mean-field phase diagrams are useful preliminaries to Monte Carlo studies. They give the nature of the local order and thus indicate which order parameters to compute. As mentioned above, for the row model, the Monte Carlo studies yielded no major changes in the $(\eta, T/J)$ phase diagram from that obtained by mean-field theory.[22] For the staggered row model, however, Monte Carlo studies using fixed periodic boundary conditions yielded a negative spin stiffness for $\eta=0.5$ and low temperatures, suggesting that the ground state of this system is incompatible with periodic boundary conditions, and hence that incommensurate phases may occur for it.[23] More careful study of the mean-field theory for the staggered row model thus became necessary; it is given in the body of the present paper. Our results are as follows.

At low temperatures, there are two ordered phases, both of them not appearing in the commensurate three-spins-per-unit-cell calculation. One is the incommensurate spiral phase with three spins per unit cell (SP3), given in Fig. 6(a) for $\eta=2$ and $T/J=0$. (Observe that the SP3 phase of the staggered row model is similar to the spiral phase of the row model.) The other is a noncollinear commensurate (NC6) phase with six spins per unit cell, given in Fig. 6(b) for $\eta=2$ and zero temperature. In the SP3 phase, the system is incommensurate with the lattice in the horizontal direction, but is periodic in the vertical direction. The phase transition between these two phases occurs only as η crosses the value 0 and is first order. At higher temperature, the SP3 phase goes continuously into either the AF phase or the FI phase found in Ref. 21, and the NC6 phase goes continuously into either the FI phase or another antiferromagnetic state (AF6), with six spins per unit cell, given in Fig. 6(c) for $\eta<0$ and $T/J=0$. (Observe that the AF6 phase of the staggered row model is similar to the AF phase of the row model.) The $(\eta, T/J)$ phase diagram is given in Fig. 7. The staggered row model is much like a combination of the row model and the centered honeycomb model: The spiral and AF phases of the row model become SP3 and AF6 in the staggered row model, and the FI and AF3 phases of the centered honeycomb model become FI and AF3 in the staggered row model. Only the NC3 phase of the centered honeycomb model does not persist

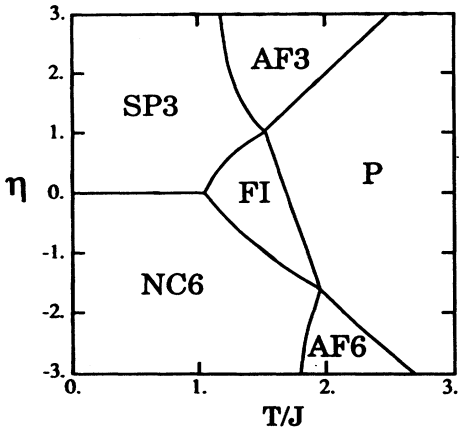

FIG. 7. Phase diagram for the staggered row model when incommensurate and six-spins-per-unit-cell solutions are included.

into the staggered row model, which nevertheless possesses the related NC6 phase.

E. Outline

A brief outline of this paper is as follows. In Sec. II, the ground state of the staggered row model is studied, and we compare the results with those for the row model. The mean-field equations are obtained in Sec. III. In Sec. IV, the solutions to the mean-field equations are obtained, and the $(\eta, T/J)$ phase diagram is given. There are five ordered phases and seven phase transition lines. In Sec. V, we study the phase-fluctuations of this system at a relatively high temperature, finding the same three transitions to the paramagnetic state as found in the previous section and finding, at the two tetracritical points, degeneracies that enable each of the two zero-temperature phases to be realized. In Sec. VI the centered honeycomb model is shown to be simply related to our previously obtained solution to the staggered row model for commensurate, three-spins-per-unit-cell solutions. Note that the centered honeycomb model, unlike the staggered row model, does not have a preferred direction and does not have a preferred wave vector and the complications associated with spiral phases. A summary is given in Sec. VII.

II. GROUND STATE OF THE STAGGERED ROW MODEL

The energy of an XY model with nearest-neighbor interactions is given by

$$E=-\sum_{\langle ij\rangle} J_{ij}\cos(\theta_i-\theta_j)\ , \tag{2.1}$$

where the sum is over the nearest-neighbor pairs. For the FFTR model, all the bonds J_{ij} equal $-J$, and the Hamiltonian has only one spin per unit cell. In the FFTR model ground state, each spin makes an angle of $2\pi/3$ (or $-2\pi/3$) with respect to its nearest neighbors. In addition to the degeneracy with respect to overall spin space rotations, this ground state of the FFTR model has a discrete twofold degeneracy, corresponding to $2\pi/3$ or $-2\pi/3$ rotations as one moves about an elementary plaquette. This is known as the *chirality* of the system.[24]

In the staggered row model, one-third of the horizontal bonds are different from the rest of the bonds, as shown in Fig. 2. Spin C has six $-J$ bonds, and spins A and B have five $-J$ bonds and one $-\eta J$ bond; so the Hamiltonian has three spins per unit cell. If $\eta>0$, all the bonds of the model are antiferromagnetic but with different strength. If $\eta<0$, one-ninth of the bonds are ferromagnetic, and the rest are antiferromagnetic.

The ground state of the staggered row model should coincide with that of the FFTR model for $\eta=1$. For $\eta>0$ the ground state is an incommensurate spiral SP3 (Sec. II A), and for $\eta<0$ the solution is a commensurate noncollinear state with six spins per unit cell NC6 (Sec. II B). Section II C discusses a numerical search for other solutions. $\eta>0$ and $\eta<0$ are treated separately.

A. $\eta>0$: Spiral with three spins per cell (SP3)

As indicated in Sec. II C, for $\eta>0$ the system goes into a spiral state with a basis of three spins, given in Fig. 6(a). Thus we search for a spiral solution, where the energy of the system is given in Eq. (2.1).

We take spin i to have a clockwise orientation angle with respect to $\hat{x}$ of

$$\theta_i=\theta_l+\Delta_x(\hat{\mathbf{x}}\cdot\mathbf{r}_i)+\Delta_y(\hat{\mathbf{y}}\cdot\mathbf{r}_i)\ , \tag{2.2}$$

where $\hat{\mathbf{x}},\hat{\mathbf{y}}$ are the unit vectors in the x and y directions, and Δ_x,Δ_y are quantities to be determined by minimizing the energy. Here, l denotes the sublattice (A, B, or C), and Δ_x and Δ_y have the physical meaning of the phase shift per site along the x and y directions. Introducing the variables

$$\begin{aligned}&\theta_0=\tfrac{1}{2}(\theta_B-\theta_A)\ ,\quad v=\theta_C-\tfrac{1}{2}(\theta_A+\theta_B)\ ,\\ &r=\cos\left[\Delta_y\frac{\sqrt{3}}{2}\right]\ ,\quad s=\cos v\ ,\end{aligned} \tag{2.3}$$

the energy per unit cell ϵ takes the form

$$\begin{aligned}\epsilon/J=&\eta\cos(2\theta_0+\Delta_x)+2r\cos(2\theta_0-\Delta_x/2)\\ &+2s[\cos(\theta_0-\Delta_x)+2r\cos(\theta_0+\Delta_x/2)]\ .\end{aligned} \tag{2.4}$$

This is minimized by the requirements that

$$\partial\epsilon/\partial\theta_A=\partial\epsilon/\partial\theta_B=\partial\epsilon/\partial\theta_C=\partial\epsilon/\partial\Delta=0\ . \tag{2.5}$$

Clearly, Eq. (2.4) is extremized by r and s each taking on the values 1 and -1, thus leading us to consider four subcases. For given values of r and s, the energy minimization conditions for θ_0 and Δ_x (henceforth called Δ), when combined, lead to

$$r\sin\left[2\theta_0-\frac{\Delta}{2}\right]+s\sin(\theta_0-\Delta)=0\ , \tag{2.6}$$

$$\eta\sin(2\theta_0+\Delta)+2rs\sin\left[\theta_0+\frac{\Delta}{2}\right]+r\sin\left[2\theta_0-\frac{\Delta}{2}\right]=0\ . \tag{2.7}$$

Detailed study shows that there are four inequivalent solutions to these equations for a given set of values for (r,s). With four sets of values for (r,s), that would lead to a total of 16 solutions. However, numerical computation shows that the same four solutions are obtained for all four sets of (r,s) by changing the domain of values for Δ. For simplicity, we thus consider only the solutions for $r=s=1$, so that $\Delta_y=v=0$. Note that $v=0$ implies that

$$\theta_0=\theta_0+v=\theta_C-\theta_A=\theta_0-v=\theta_B-\theta_C \ . \tag{2.8}$$

In this case, the appropriate solution to Eq. (2.6) is

$$\theta_0=\frac{2\pi}{3}+\frac{\Delta}{2} \ . \tag{2.9}$$

This leads to

$$\eta=-\frac{2\sin(2\pi/3+\Delta)+\sin(4\pi/3+\Delta/2)}{\sin(4\pi/3+2\Delta)} \ . \tag{2.10}$$

Equation (2.10) is periodic in Δ, with period 4π, and is symmetric under the transformation $\Delta\rightarrow(2\pi/3-\Delta)$. With Eq. (2.9) and $r=s=1$, the energy per unit cell of Eq. (2.4) becomes

$$\epsilon/J=\eta\cos\left[\frac{4\pi}{3}+2\Delta\right]+4\cos\left[\frac{2\pi}{3}-\frac{\Delta}{2}\right]+4\cos\left[\frac{2\pi}{3}+\Delta\right] , \tag{2.11}$$

where $-\pi/6<\Delta<\pi/3$. For $\Delta=0$, the solution given by Eq. (2.10) gives the FFTR model result that $\eta=1$ and $\theta_B-\theta_C=2\pi/3$. By continuity, we expect this to be the correct solution in the vicinity of $\eta=1$. [Note that, for $\eta=0$, Eq. (2.10) implies that $\cos(\pi/3+\Delta/4)=1/4$, so that Eq. (2.11) then yields $\epsilon/J=-4.5$, a result that will be employed in the next section.] Values of Δ outside the domain $(-\pi/6,\pi/3)$ yield either a repeating branch of the above solution or two branches of the other three solutions, whose energies are higher, for all values of η. (The highest-energy solution occurs only for $\eta<-3/4$; the second highest-energy solution occurs only for $\eta<-5/4$; the third highest-energy solution occurs only for $\eta>\eta_0$, where $\eta_0\approx2.2356$.) From Eq. (2.10) it follows that as $\eta\rightarrow+\infty$, $\Delta\rightarrow-\pi/6$, and in each cell spins A and B point in opposite directions. The relation between η and Δ is shown in Fig. 8. For $\eta<0$ the phase shift is given as zero. Here the system is in the commensurate NC6 state ($\Delta=0$), which occurs by a first-order transition.

For finite temperature, the "lengths" of the spins on each sublattice change with temperature, as does Δ. If the temperature is high enough, the spiral, or helical, states disappear. We discuss this in the next section.

There are several other, higher-energy, solutions of Eqs. (2.6) and (2.7), such as

$$\theta_0=\pi \ , \quad \Delta=0 \tag{2.12}$$

and

$$\theta_0=\frac{2\pi}{3} \ , \quad \Delta=\frac{2\pi}{3} \ . \tag{2.13}$$

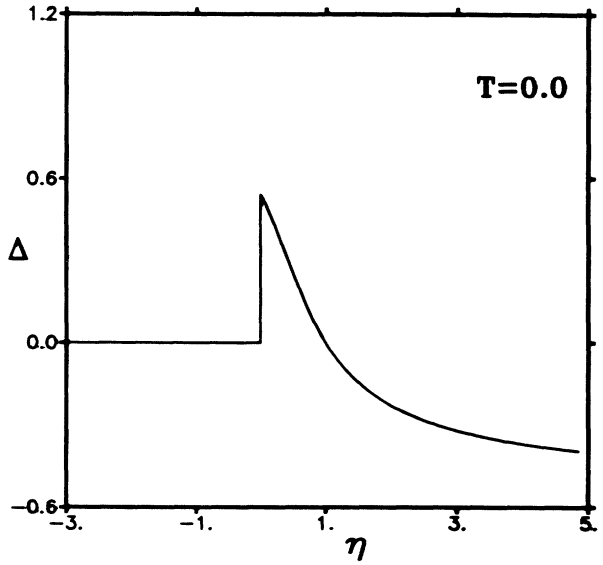

FIG. 8. Δ vs η at $T=0$ for the staggered row model.

The energy per unit cell for each of these states is $\epsilon/J=-4+\eta$. Equation (2.12) describes the FI state, and Eq. (2.13) describes the AF3 state. These phases appear at finite temperature. As $\eta\rightarrow-\infty$, the energy difference between these states and the ground state goes to zero.

If one takes the approach of requiring each spin to point along the direction of its local field and takes $\Delta_y=v=0$, the symmetry of the solution guarantees both that spin C points along its local field and that the condition for spin B then reduces to that for spin A. It is still necessary to minimize the energy with respect to the pitch Δ.

B. $\eta<0$: Commensurate noncollinear state with six spins per cell (NC6)

As indicated in Sec. II C, for $\eta<0$ the system goes into the commensurate noncollinear state with six spins per unit cell (NC6) given in Fig. 6(b). For $\eta<0$ there is a ferromagnetic interaction between spins A and B in the $\hat{\mathbf{x}}$ direction, which causes spins A and B to tip together. (If one considers A and B to act as a single spin, the triangular lattice reduces to a square lattice with two different kinds of spins, four spins per unit cell, and a commensurate ground state.)

Let the spins in the odd rows make an angle of θ_l' with the horizontal axis and the spins in the even rows make an angle of $-\theta_l'$, where l may be A, B, or C. We take $\theta_A'=\theta_B'$. Note that θ_B' is defined counterclockwise with respect to $\hat{\mathbf{x}}$, whereas θ_C' is defined clockwise with respect to $-\hat{\mathbf{x}}$. See Fig. 6(b). Either by minimizing the energy or by requiring that spins B and C point along their local fields (the condition for A is the same as for B), we obtain

$$\sin(\theta_C'-\theta_B')-2\sin(\theta_B'+\theta_C')-\sin(2\theta_B')=0 \ , \tag{2.14}$$

$$\sin(\theta_B'-\theta_C')-2\sin(\theta_B'+\theta_C')=0 \ . \tag{2.15}$$

Their solution is

$$\tan\theta'_B = \mp\sqrt{\tfrac{5}{3}} , \tag{2.16}$$

$$\tan\theta'_C = \pm\sqrt{\tfrac{5}{27}} , \tag{2.17}$$

with energy per cell

$$\epsilon/J = -4.5+3\eta . \tag{2.18}$$

These solutions are independent of η, and the energy is a linear function of η. This is because, for $\eta<0$, spins A and B couple together and the spin configuration is decided by the $-J$ bonds.

For $\eta=0$, the NC6 state has the same energy as the SP3 state, but a totally different spin configuration. Thus, if η changes from positive to negative, the system undergoes a first-order transition.

C. Search for other solutions

Because this spin system proved to be rather complex, to confirm the analytical results we also studied this system by purely numerical methods. Assuming that the ground state is a type of six-spin incommensurate spiral state, we set six spins per unit cell and varied the boundary condition by adding a phase shift Δ. For 12, 24, and 36 spins per unit cell, we found that when $\eta>0$ the three spin spiral state SP3 has the lowest energy and when $\eta<0$ the commensurate noncollinear six-spin state NC6 has the lowest energy.

Note that other methods to find the ground state of complex systems have also also been employed.[25–28] We employ a related method in Sec. V.

III. MEAN-FIELD EQUATIONS FOR FINITE TEMPERATURE

The partition function is given by

$$Z=\int_{-\pi}^{\pi}\prod_i (d\theta_i)\exp[-\beta H(\mathbf{S}_i)] , \tag{3.1}$$

where $\beta=T^{-1}$, and we employ units in which the Boltzmann constant $k_B=1$. The free energy is

$$F=-\frac{1}{\beta}\ln Z . \tag{3.2}$$

Using the mean-field approximation

$$\mathbf{S}_i\cdot\mathbf{S}_i \rightarrow \langle\mathbf{S}_i\rangle\cdot\mathbf{S}_i+\mathbf{S}_i\cdot\langle\mathbf{S}_i\rangle-\langle\mathbf{S}_i\rangle\cdot\langle\mathbf{S}_i\rangle , \tag{3.3}$$

the free energy F is given by

$$F=-\sum_{\langle ij\rangle} J_{ij}\langle\mathbf{S}_i\rangle\cdot\langle\mathbf{S}_i\rangle-\frac{1}{\beta}\sum_i \ln\left[\int_{-\infty}^{\pi} d\theta_i \exp(\beta\mathbf{H}_i\cdot\mathbf{S}_i)\right], \tag{3.4}$$

where the local field is written as

$$\mathbf{H}_i=\sum_{\langle j\rangle} J_{ij}\langle\mathbf{S}_j\rangle , \tag{3.5}$$

and the summation $\langle j\rangle$ is over the nearest neighbors of site i. Minimizing the free energy requires that $\langle\mathbf{S}_i\rangle$ have the same direction as the local field $\mathbf{H}_i$ and

$$S_i=R(\beta H_i) , \tag{3.6}$$

where $S_i=|\langle\mathbf{S}_i\rangle|$ is the "length" of the ith spin, and H_i is the strength of local field at site i. The function $R(u)$ is

$$R(u)=\frac{\int_{-\pi}^{\pi} e^{u\cos\theta}\cos\theta\, d\theta}{\int_{-\pi}^{\pi} e^{u\cos\theta} d\theta}=\frac{I_1(u)}{I_0(u)} , \tag{3.7}$$

where $I_n(u)$ is a modified Bessel function of order n. $R(u)$ has the properties that $R(u)\rightarrow 1$ as $u\rightarrow\infty$, and $R(u)\rightarrow u/2$ as $u\rightarrow 0$. As for the ground states, the cases $\eta>0$ and $\eta<0$ are studied separately.

A. Mean-field equations for $\eta>0$

The ground state for $\eta>0$ is the incommensurate spiral state SP3. Near zero temperature, the system remains in the spiral state. Let S_i and θ_i be the length and orientation of the spin at site i. As for the ground state, we choose θ_i as

$$\theta_i=\theta_l+\Delta(\hat{\mathbf{x}}\cdot\mathbf{r}_i) . \tag{3.8}$$

where l may be one of A, B, C and Δ is to be determined by minimizing the free energy. In this case, spins on the same sublattice have the same lengths but point in different directions, and spins on different sublattices have different lengths. Each spin has the same direction as the local field $\mathbf{H}_i$. We rewrite the free energy as

$$F=-E-\frac{1}{\beta}\sum_i \ln\left[\int_{-\pi}^{\pi}\exp(\beta H_i\cos\theta_i)d\theta_i\right] , \tag{3.9}$$

where E, the average energy of the system, is given by

$$E=-\frac{1}{2}\sum_i \mathbf{H}_i\cdot\langle\mathbf{S}_i\rangle=-\sum_{\langle ij\rangle} J_{ij}S_iS_j\cos(\theta_i-\theta_j) . \tag{3.10}$$

Minimizing the free energy with respect to Δ, we obtain

$$\frac{\partial F}{\partial\Delta}=-\frac{\partial E}{\partial\Delta}-\sum_i\frac{\partial H_i}{\partial\Delta}R(\beta H_i)=0 , \tag{3.11}$$

which leads to

$$S_A\frac{\partial H_A}{\partial\Delta}+S_B\frac{\partial H_B}{\partial\Delta}+S_C\frac{\partial H_C}{\partial\Delta}=0 . \tag{3.12}$$

In the present case the symmetry between sublattices A and B can be used to simplify the problem. We take $S_A=S_B=B$ and $S_C=C$, and $v=0$ in Eq. (2.3); so use of Eq. (2.8) gives $\theta_B-\theta_C=\theta_C-\theta_A=\theta_0$. The mean-field equations then become

$$B\sin\left[2\theta_0-\frac{\Delta}{2}\right]+C\sin(\theta_0-\Delta)=0 , \tag{3.13}$$

$$\eta B\sin(2\theta_0+\Delta)+2C\sin\left[\theta_0+\frac{\Delta}{2}\right]+B\sin\left[2\theta_0-\frac{\Delta}{2}\right]=0 , \tag{3.14}$$

where Eq. (3.13) arises from Eq. (3.12), and Eq. (3.14) arises from the condition that spin B point along its local field. Moreover, by Eq. (3.6)

$$B=R(\beta H_B) , \quad C=R(\beta H_C) , \tag{3.15}$$

where the local fields H_B and H_C obtained from Eq. (3.5) are given by

$$H_B/J=|C\cos(\theta_0-\Delta)+2C\cos(\theta_0+\Delta/2)+2B\cos(2\theta_0-\Delta/2)+\eta B\cos(2\theta_0+\Delta)| \ . \tag{3.16}$$

$$H_C/J=|2B\cos(\theta_0-\Delta)+4B\cos(\theta_0+\Delta/2)| \ , \tag{3.17}$$

Near zero temperature, where $\beta\to\infty$, $R(\beta H_i)=1$, and Eqs. (3.13) and (3.14) reduce Eqs. (2.6) and (2.7) for the ground state when $r=s=1$.

B. Mean-field equations for $\eta<0$

The ground state for $\eta<0$ is the commensurate noncollinear six-spin state NC6. Near zero temperature, the system will remain in this state. As in the case of the ground state, we let spins in one row have angles of θ_i' and spins in adjacent rows have angles of $-\theta_i'$, where i may be A, B, or C, and we set $\theta_A'=\theta_B'$. As in Sec. II B, θ_B' is defined counterclockwise with respect to $\hat{\mathbf{x}}$, and θ_C' is defined clockwise with respect to $-\hat{\mathbf{x}}$. Again, see Fig. 6(b).

Requiring each spin to point along its local field $\mathbf{H}_i$, the equations for B and C are

$$C\sin(\theta_C'-\theta_B')-2C\sin(\theta_B'+\theta_C')-B\sin(2\theta_B')=0 \ , \tag{3.18}$$

$$\sin(\theta_B'-\theta_C')-2\sin(\theta_B'+\theta_C')=0 \ . \tag{3.19}$$

At zero temperature, $B=C=1$, and the above equations reduce to Eqs. (2.14) and (2.15) for the ground state. Note that (3.19) is the same as (2.15). Away from zero temperature, the spin lengths and the spin angles θ_B' and θ_C' depend on both η and temperature. Equations (3.18) and (3.19) can be rewritten as

$$B\sin\theta_B'=2C\sin\theta_C' \ , \tag{3.20}$$

$$\tan\theta_B'=-3\tan\theta_C' \ . \tag{3.21}$$

Moreover, by Eq. (3.6),

$$B=R(\beta H_B) \ , \quad C=R(\beta H_C) \ , \tag{3.22}$$

where the local fields H_B and H_C obtained from Eq. (3.5) are given by

$$H_B/J=|-B\eta+C\cos(\theta_B'+\theta_C')+2C\cos(\theta_B'-\theta_C')-2B\cos(2\theta_B')| \ , \tag{3.23}$$

$$H_C/J=|4B\cos(\theta_C'+\theta_B')+2B\cos(\theta_C'-\theta_B')| \ . \tag{3.24}$$

Note that Eq. (3.21) is valid at all temperatures. From Eqs. (3.13)–(3.17) and Eqs. (3.20)–(3.24), a rich phase diagram is obtained, as discussed in the next section.

IV. PHASE DIAGRAM FOR THE STAGGERED ROW MODEL

A. $\eta>0$: SP3 phase and the SP3-AF3, SP3-FI transitions

For $\eta>1$, the bond $-\eta J$ tends to orient A and B oppositely, and gives them mean fields larger than for spin C. As the temperature is increased, the mean field seen by spin C is overwhelmed by the thermal energy, and thus spin C "melts," and so $C\to 0$. At the same time, A and B becomes completely opposed to one another, and so $\theta_0\to\pi/2$, and the system leaves the spiral state, and so $\Delta\to 0$. The system then enters the antiferromagnetic state AF3, in which spins A and B are opposed.

We now obtain the phase transition line between SP3 and AF3. From the above discussion, near this transition $\{C,\Delta,\theta'=\theta_0-\pi/2\}$ are small. Only the first-order terms of Eqs. (3.13)–(3.17) are important. They are

$$-B\left[2\theta'-\frac{\Delta}{2}\right]+C=0 \ , \tag{4.1}$$

$$-\eta B(2\theta'+\Delta)+2C-B\left[2\theta'-\frac{\Delta}{2}\right]=0 \ , \tag{4.2}$$

$$B=R(\beta H_B) \ , \quad C=R(\beta H_C)\approx\beta H_C/2 \ , \tag{4.3}$$

$$H_B/J\approx(2+\eta)B \ , \quad H_C/J\approx 6B\theta' \ . \tag{4.4}$$

The transition line is found by solving four of the above equations [only the last half of Eqs. (4.3) and (4.4) are needed], leading to

$$T_c/J=1+\frac{1}{2\eta}(\text{SP3-AF3 line}) \ , \tag{4.5}$$

where, for $\eta=1$, $T_c/J=1.5$, and as $\eta\to+\infty$, $T_c\to 1$. Expanding Eqs. (3.13)–(3.17) to higher order, one can show that $\Delta\propto\sqrt{T_c-T}$ near the SP3-AF3 transition line.

Numerical results, based on Eqs. (3.13)–(3.17), are shown in Fig. 9, for $\eta=2$. In Fig. 9(a), the relation between Δ and temperature is given. Δ is negative for the special spin configuration we choose. In Fig. 9(b), the relation between θ_0 and temperature is given. As $T\to T_c$, $\theta_0\to\pi/2$, as expected.

For $0<\eta<1$, the bond $-\eta J$ repelling spins A and B is weak. Because of the stronger repulsion of spin C, there is an effective attraction between spins A and B in the same cell, and so they tend to tip together and form a spin pair. In this case, the weakest mean field in the problem is the transverse component of the fields on spins A and B. As the temperature is increased, the thermal energy overwhelms this mean field, and the system enters a collinear state where spins A and B have equal lengths and are opposed to spin C. Following Ref. 21, we denote this state, with a net magnetic moment, as FI.

To obtain the transition line between SP3 and FI, we note that to get the FI state from the SP3 state, we may take $\Delta\to 0$ and $\theta_0\to\pi$ in Eqs. (3.13)–(3.17). Then Eqs. (3.13) and (3.14) combine to yield an equation that holds only along the SP3-FI line:

$$\frac{C}{B}=\frac{1}{2}(\eta+3/2)+\frac{1}{2}\sqrt{(\eta+3/2)^2-4\eta} \quad \text{(SP3-FI line)} . \tag{4.6}$$

In addition, Eqs. (3.13)–(3.17) combine to yield

$$B=R[3\beta JC-(2+\eta)\beta JB] \quad \text{(FI phase)} , \tag{4.7}$$

$$C=R(6\beta JB) \quad \text{(FI phase)} , \tag{4.8}$$

which hold throughout the FI phase. The SP3 to FI phase transition line must be obtained numerically from the above three equations. If $\eta=1$, then $C/B=2$ and $T_c/J=1.5$, consistent with the FFTR model. Note that the SP3-AF3 and AF3-FI lines come together at $\eta=1, T_c/J=1.5$. For $\eta=0.5$ the relation between the phase shift Δ and temperature is given in Fig. 10(a), where Δ is positive. Near the transition line, $\Delta\propto\sqrt{T_c-T}$, and so $\Delta\to 0$, as expected. The phase transition from SP3 to FI is of second order. For $\eta=0.5$ the relation between the angle θ_0 and temperature is given in Fig. 10(b). Near the transition line $\theta_0\to\pi$, as expected.

B. $\eta>0$: AF3 phase and the AF3-P transition

In the AF3 phase, spin C melts, spins A and B have equal length and they are in opposite directions, as shown in Fig. 2(a), and, so the system has an antiferromagnetic ordering. With $C=0$, $\Delta=0$, and $\theta_0=\pi/2$, Eq. (2.4) yields

$$H_B=(2+\eta)B , \quad B=R(\beta H_B) \quad \text{(AF3 phase)} . \tag{4.9}$$

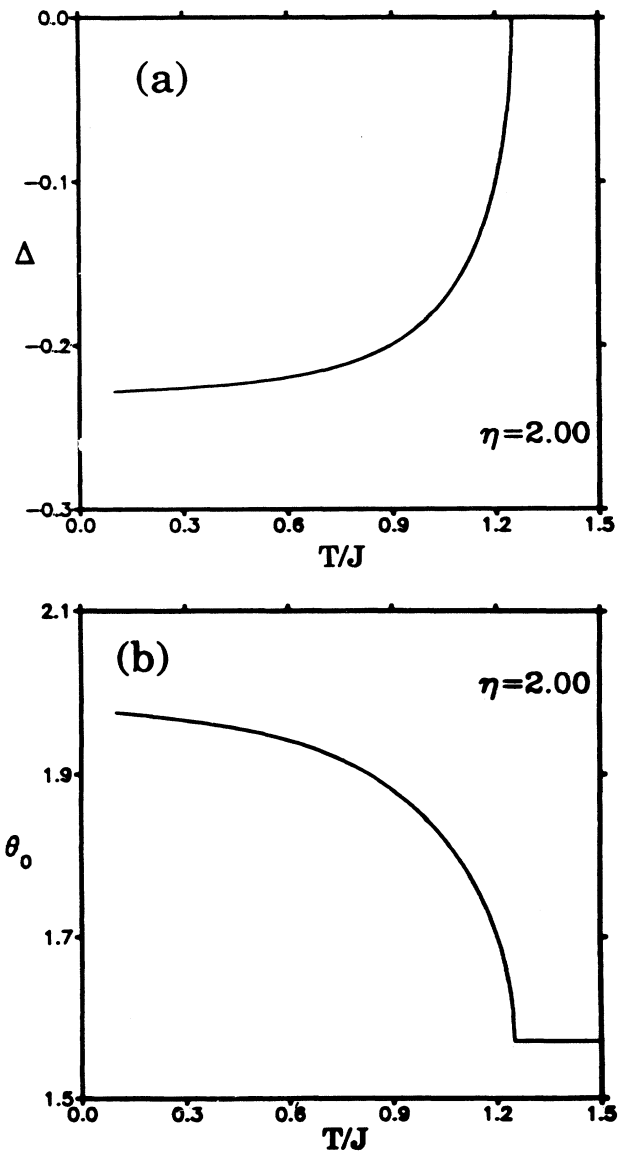

FIG. 9. (a) Δ vs T, (b) θ_0 vs T.

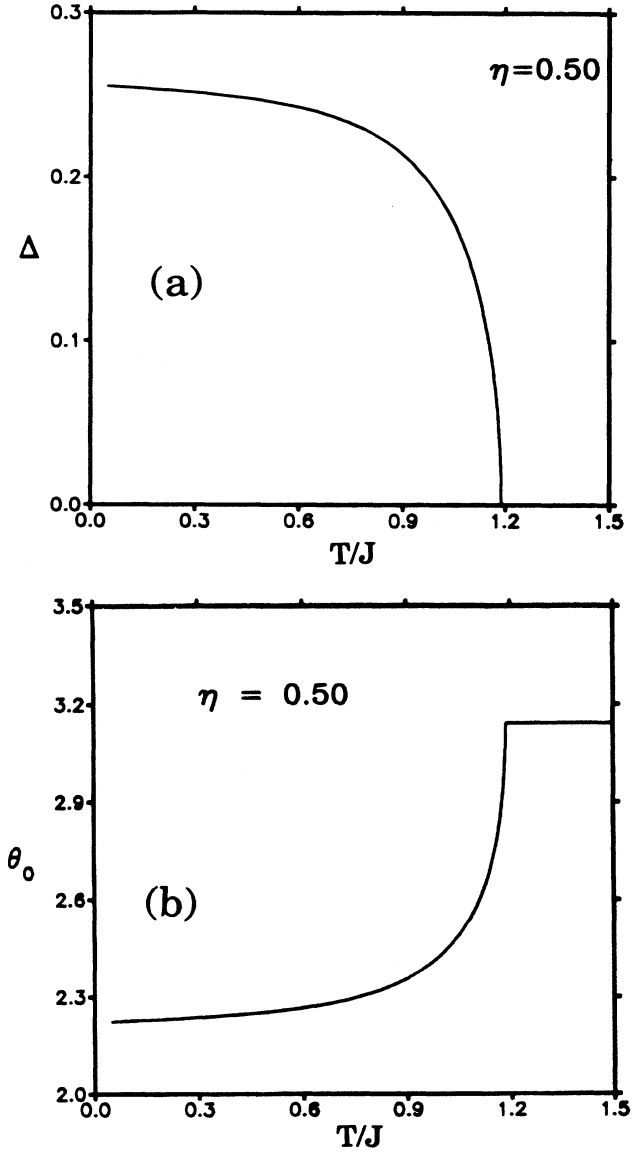

FIG. 10. (a) Δ vs T, (b) θ_0 vs T.

From the AF3 state, if the temperature goes still higher, the spins on all sites will melt. Near the transition line of AF3 to P, B is small, and so

$$B=R(\beta H_B)\rightarrow\beta H_B/2 \quad (\text{AF3-}P \text{ line}) . \tag{4.10}$$

From Eqs. (4.9) and (4.10) the AF3-P transition line is given by

$$T_c/J=1+\frac{\eta}{2} \quad (\text{AF3-}P \text{ line}) . \tag{4.11}$$

For $\eta=1, T_c/J=1.5$. Thus the AF3-P line meets the SP3-AF3 and SP3-FI lines at $\eta=1$, $T_c/J=1.5$. For $\eta\rightarrow\infty$, $T_c\propto\eta/2$. This phase transition is second order.

C. FI phase and the FI-P transition

In the FI state, spins A and B are in the same direction, and point oppositely to C. The system is described by Eqs. (4.7) and (4.8). The system has a net magnetization

$$M=\left|\frac{1}{N}\sum_i\langle \mathbf{S}_i\rangle\right|=\frac{(2B-C)}{3} , \tag{4.12}$$

Approaching the FI-P transition temperature from below, the spin lengths approach zero, and so Eq. (3.5) yields

$$B=R(\beta_c H_B)\rightarrow\beta_c H_B/2, C=R(\beta_c H_C)\rightarrow\beta_c H_C/2 . \tag{4.13}$$

With Eq. (4.13), Eqs. (4.7) and (4.8) yield

$$T_c/J=\tfrac{1}{4}[\sqrt{(2+\eta)^2+72}-(2+\eta)] \quad (\text{FI-}P \text{ line}) . \tag{4.14}$$

$T_c/J=1.5$ if $\eta=1$, as expected. Thus the FI-P line meets the SP3-FI and AF3-P lines at $\eta=1, T_c/J=1.5$. The phase transition between the FI state and paramagnetic state is of second order. Note that (4.14) also holds for $\eta<0$, and that $T_c/J=2$ for $\eta=-1.5$.

D. $\eta<0$: NC6 phase and the NC6-FI, NC6-AF6 transitions

The six-spin noncollinear state NC6 is a commensurate state, described by Eqs. (3.20)–(3.24). In this state, spins A and B are always coupled together, and the system has a net magnetization

$$M=\left|\frac{2B\cos\theta'_B-C\cos\theta'_C}{3}\right| . \tag{4.15}$$

Using Eqs. (3.20) and (3.21), we have

$$M=\left|\frac{B\cos\theta'_B}{6}\right| . \tag{4.16}$$

Because the spin configurations of the NC6 and SP3 phases do not go into one another continuously, the NC6-SP3 phase transition is first order. Using Eq. (3.9), the free energy has been evaluated numerically. For $\eta>0$, the SP3 state has the lower free energy; for $\eta<0$, the NC6 state has the lower free energy. Despite its first-order character (in the sense of a change in symmetry), there seems to be no hysteresis. See Fig. 7 for the phase transition line.

In the NC6 state, two kinds of interaction compete with one other. One is between the nearest spin pair AB, and the other is between the pair AB and its neighbor, spin C.

For $0>\eta>-1.5$, the local field of spin C is much stronger than that of spin A and spin B. In that case the interaction between spin C and the nearest AB pairs dominates, and the AB pairs point opposite to spin C. The system thus goes from the NC state to the FI state. Near the phase transition from the NC6 state to the FI state, $\theta'_B\rightarrow0$ and $\theta'_C\rightarrow\pi$ in Eqs. (3.20)–(3.24). The NC6-FI phase transition line is found by solving Eqs. (4.7) and (4.8) for the FI state, along with the condition that

$$3B=2C \quad (\text{NC6-FI line}) , \tag{4.17}$$

which follows from Eqs. (3.20) and (3.21). The NC6-FI line is shown in Fig. 7. This phase transition is of second order. Note that letting $B,C\rightarrow0$ gives a solution for $\eta=-1.5, T_c/J=2$.

For $\eta\ll-1$, due to the strong bond $-\eta J$, the local field of spin A and spin B is much stronger than that of spin C, and so the length of spin A and spin B is greater than that of spin C, and the AB pair interaction dominates. As the temperature increases, the system enters the AF6 state, where nearest spin pairs point in the opposite direction. This spin configuration is given in Fig. 6(c), where all the spins in each row point in one direction and all the spins in the next row point in the opposite direction. Near the phase transition from the NC6 state to the AF6 state, $\theta'_B\rightarrow\pi/2, \theta'_C\rightarrow\pi/2$, and so by Eq. (3.20),

$$B\rightarrow2C \quad (\text{NC6-AF6 line}) . \tag{4.18}$$

The NC6-AF6 phase transition line is found by employing Eq. (4.18) in solving

$$B=R(\beta H_B)=R\{\beta J[C+(2-\eta)B]\} \quad (\text{AF6 phase}) , \tag{4.19}$$

$$C=R(\beta H_C)=R(2\beta JB) \quad (\text{AF6 phase}) , \tag{4.20}$$

which follow from Eqs. (3.22) and (3.24), and hold throughout the AF6 phase. The NC6-AF6 line is shown in Fig. 7. This phase transition is of second order. Note that letting $B,C\rightarrow0$ gives a solution for $\eta=-1.5, T_c/J=2$.

E. $\eta<0$: AF6 phase and the AF6-P transition

In the AF6 state, spins in the same row have the same direction, and each unit cell has six spins. At higher temperatures, the AF6 state is not stable, and the system enters the paramagnetic (P) state. This phase transition is of second order. By the previous subsection, the AF6 state is described by Eqs. (4.19) and (4.20). As the system enters the P state, $B,C\rightarrow0$, and so with $R(x)\approx x/2$ for small x, Eqs. (4.19) and (4.20) give the AF6-P phase transition line as

$$T_c/J=\tfrac{1}{4}[(2-\eta)+\sqrt{(2-\eta)^2+8}] \quad \text{(AF6-}P\text{ line)} . \tag{4.21}$$

For $\eta=-1.5$, this gives $T_c/J=2$. As a consequence, the AF6-P and FI-P lines meet at this point. This is a tetracritical point because, from our earlier discussion, the NC6 phase also meets at this point.

Note that, as $\eta\to-\infty, T_c/J\to-\eta/2$.

V. FLUCTUATION ANALYSIS AT FINITE TEMPERATURE

It is well known that fluctuations play an important role in two dimensions. In particular, they tend to sizably depress the value of the critical temperature deduced from mean-field theory. This feature allows, in addition to the treatment given above, an approximate treatment known as the phase-only approach: The amplitude of the order parameter is fixed, and only fluctuations of the phase about the mean-field solution are taken into account. The starting point of this procedure consists in identifying the critical modes in the $(\eta, T/J)$ phase diagram. For $\eta\neq1$, the periodicity in the horizontal direction is changed, making the unit cell 3 times as large, resulting in a new Brillouin zone that is one-third as large. Both old and new Brillouin zones are shown in Fig. 11. It defines the manifold of wave vectors $\mathbf{q}$ used to construct a Landau-Ginzburg-Wilson expansion derived from the Hamiltonian [Eq. (2.1)]. Following a standard procedure (Refs. 21 and 29), one can show that, near criticality, the functional free energy F, which includes a factor β so that it is dimensionless, is given in terms of the exchange matrix $\mathscr{J}$ and the critical mode fluctuations Ψ by

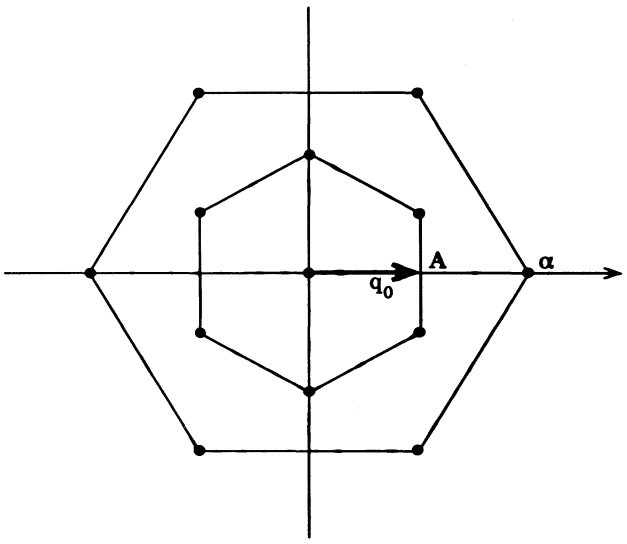

FIG. 11. Brillouin zones for the row model (larger hexagon) and for the staggered row model (smaller hexagon). The points α and A have coordinates $(4\pi/3,0)$ and $(2\pi/3,0)$, respectively, where the nearest-neighbor distance has been set to unity.

$$F\{\Psi_{\mathbf{q}}\}=F_0+\frac{1}{2}\sum_{\mathbf{q}}\Psi_{\mathbf{q}}\cdot[\{\beta\mathscr{J}_{\mathbf{q}}\}^{-1}-(1/2)\cdot\mathbf{1}]\cdot\Psi_{\mathbf{q}}^{*}+O(\Psi_{\mathbf{q}}^{4}) \tag{5.1}$$

where

$$\Psi_{\mathbf{q}}=(\Psi_{\mathbf{q}}^{A},\Psi_{\mathbf{q}}^{B},\Psi_{\mathbf{q}}^{C}) \tag{5.2}$$

and $\Psi_{\mathbf{q}}^{A}$ is a two-dimensional vector in spin space, proportional to $S_x^A(\mathbf{q})+iS_y^A(\mathbf{q})$. Here, $\mathscr{J}_{\mathbf{q}}$ is the $\mathbf{q}$ space representation of the exchange matrix coupling these sublattices, explicitly given by

$$\mathscr{J}_{\mathbf{q}}=-J\begin{bmatrix}0 & a & b^{*}\\ a^{*} & 0 & b\\ b & b^{*} & 0\end{bmatrix}, \tag{5.3}$$

with

$$a=\eta\exp(i\mathbf{q}_x)+2\exp(-iq_x/2)\cos(q_y\sqrt{3}/2) , \tag{5.4}$$

$$b=\exp(iq_x)+2\exp(-iq_x/2)\cos(q_y\sqrt{3}/2) . \tag{5.5}$$

The critical lines $T_c(\eta)$ separating the paramagnetic state from the ordered phases are obtained by demanding that the largest eigenvalue of $\{\beta\mathscr{J}_{\mathbf{q}}\}^{-1}-(1/2)\cdot\mathbf{1}$ equal zero. In addition to yielding T_c, this approach also determines the real-space configuration of the system, by Fourier transform.

As we show below, two situations are encountered: Either the critical modes lead to configurations with equal spin amplitudes on the three sublattices and the solutions are acceptable at all temperature (this occurs only for $\eta=1$ and $\eta=-1.5$), or the amplitudes are unequal, which implies additional transitions at lower temperatures, since the ground state must have equal amplitudes on all sites. This is indeed the case, as seen from Fig. 7 and Ref. 21.

There are three regimes: $\eta>1, -1.5<\eta<1$, and $\eta<-1.5$. We analyze each of these cases, and then consider the special points $\eta=1$ and $\eta=-1.5$.

A. $\eta>1$ (AF3-P transition)

For $\eta>1$, the largest eigenvalue of $\mathscr{J}, J_{\max}(\mathbf{q})$, occurs at $\mathbf{q}=\mathbf{0}$, with

$$T_c=J_{\max}(\mathbf{0})/2=(1+\eta/2)J . \tag{5.6}$$

This corresponds to Eq. (4.11), which describes the AF3-P phase transition. The corresponding eigenvector, from Eq. (5.2), is $\mathbf{V}_1=(-1,1,0)$, which indeed corresponds to AF3 order. The critical mode is given in real space by

$$\Psi^{A}=-A\exp i\theta , \quad \Psi^{B}=A\exp i\theta , \quad \Psi^{C}=0 , \tag{5.7}$$

where θ reflects the overall rotational invariance.

Because $|\Psi^C|\neq|\Psi^A|=|\Psi^B|$, this solution cannot describe the ground state at $T=0$, where all the spins must take the same (unit) length.

B. $-1.5<\eta<1$ (FI-P transition)

Once again $J_{\max}(\mathbf{q})$ occurs at $\mathbf{q}=\mathbf{0}$, with

$$T_c = J_{\max}(\mathbf{0})/2 = \frac{\sqrt{(2+\eta)^2+72}-(2+\eta)}{4} J \ . \quad (5.8)$$

This is the same as Eq. (4.15), which describes the FI-P phase transition. The corresponding eigenvector, from Eq. (5.2), is $\mathbf{V}_2=(-1,-1,\gamma)$, with $\gamma=\frac{1}{6}[\sqrt{(2+\eta)^2+72}+(2+\eta)]$, and the critical mode is given in real space by

$$\Psi^A = -A \exp i\theta \ , \quad \Psi^B = -A \exp i\theta \ , \quad \Psi^C = \gamma A \exp i\theta \ . \quad (5.9)$$

As in the previous case, this solution cannot represent the $T=0$ configuration of the system.

C. $\eta < -1.5$ (AF6-P transition)

In this case, $J_{\max}(\mathbf{q})$ occurs at $\mathbf{q}=\mathbf{q}_0=(2\pi/3,0)$ (see Fig. 11), with

$$T_c = \tfrac{1}{4}[(2-\eta)+\sqrt{(2-\eta)^2+8}]J \ . \quad (5.10)$$

This is the same as Eq. (4.21), which describes the AF6-P transition. The corresponding eigenvector, from Eq. (5.2), is $\mathbf{V}_3=(1,\exp -i2\pi/3, \ \gamma' \exp i2\pi/3)$, with $\gamma'=\frac{1}{2}[\sqrt{(2-\eta)^2+8}-(2-\eta)]$. Once again, this solution cannot represent the $T=0$ configuration of the system.

From the standpoint of critical fluctuations, the above three cases, each involving only a single wave vector, are all in the same universality class as the ferromagnetic XY mode in 2D. There is only a single wave vector in the last case because $\mathbf{q}_0$ and $-\mathbf{q}_0$ are equivalent in the new Brillouin zone ($2\mathbf{q}_0$ is one of the reciprocal-lattice vectors of the new Brillouin zone) and because the "star" of wave vectors equivalent to $\mathbf{q}_0$ only contains $\mathbf{q}_0$ for $\eta \neq 1$ (rotational invariance has been broken). See Fig. 11.

D. Special point $\eta=1$

In this case, the eigenvectors $\mathbf{V}_1=(-1,1,0)$ and $\mathbf{V}_2=(-1,-1,2)$ become degenerate, with common eigenvalue $J_{\max}=3J$, and so $T_c=J_{\max}/2=1.5J$. Thus we may construct the linear combination

$$\left[\exp i\frac{2\pi}{3}+\frac{1}{2}\exp -i\frac{2\pi}{3}\right]\mathbf{V}_1+\left[\frac{1}{2}\exp -i\frac{2\pi}{3}\right]\mathbf{V}_2 = \left[1,\exp i\frac{2\pi}{3},\exp -i\frac{2\pi}{3}\right] , \quad (5.11)$$

leading to

$$\Psi^A = A \exp i\theta \ , \quad \Psi^B = A \exp i\left[\theta+\frac{2\pi}{3}\right] , \quad \Psi^C = A \exp i\left[\theta-\frac{2\pi}{3}\right] . \quad (5.12)$$

This form has equal amplitude for each spin and thus, with the amplitude growing from zero to unity as one moves from the tetracritical point to $T=0$, one has a solution acceptable even at $T=0$. Indeed, it is precisely the spiral solution SP3 of our previous analysis.

E. Special point $\eta=-1.5$

In this case, the eigenvectors $\mathbf{V}_2$ and $\mathbf{V}_3$, which correspond to different wave vectors, become degenerate, with common eigenvalue $J_{\max}=4J$, and so $T_c=J_{\max}/2=2J$. This degeneracy at different wave vectors is exactly what happens for $\eta=1$ in the generalized Villain model.[21] In the present case, the unit cell of the mode is doubled (to six spins per cell) relative to the unit cell of the Hamiltonian, and it is therefore easier to enlarge the space of the modes accordingly:

$$\Psi_{\mathbf{q}}=(\Psi_{\mathbf{q}}^A,\Psi_{\mathbf{q}}^B,\Psi_{\mathbf{q}}^C,\Psi_{\mathbf{q}}^{A'},\Psi_{\mathbf{q}}^{B'},\Psi_{\mathbf{q}}^{C'}) \ . \quad (5.13)$$

This amounts to a further decrease in the size of the Brillouin zone. In this space, we find that $J_{\max}(\mathbf{0})=4J$ is associated with the two independent, nonorthogonal eigenvectors $\mathbf{W}_1=(2,2,-3,2,2,-3)$ and $\mathbf{W}_2=(-2,-2,-1,2,2,1)$. Thus we may construct the linear combination

$$a\mathbf{W}_1+b\mathbf{W}_2 \ , \quad a=\frac{-19+i\sqrt{15}}{32} \ , \quad b=\frac{-5-3i\sqrt{15}}{32} \ . \quad (5.14)$$

As with Eq. (5.2), applicable to $\eta=1$, Eq. (5.14) has equal amplitude for each spin. Thus, with the amplitude growing from zero to unity as one moves from the tetracritical point to $T=0$, one has a solution acceptable even at $T=0$. Indeed, it is precisely the solution NC6 of our previous analysis.

For both $\eta=1$ and $\eta=-1.5$, two modes are degenerate. (For $\eta=-1.5$, only two modes are degenerate because rotational invariance is broken for all $\eta \neq 1$.) Therefore the phase-only analysis of fluctuations for $\eta=1$ and $\eta=-1.5$ will lead to the same critical behavior, namely, a mixture of Ising and XY character. Choi and Doniach[29] obtained a similar situation for a flux per plaquette of π and $\pi/2$. For the present case, we note that, for $\eta<0$, only 2/3 of the plaquettes are frustrated, so that systems with flux per plaquette of π and $2\pi/3$ belong to the same universality class.

VI. CENTERED HONEYCOMB MODEL

Our treatment will be brief, since the results can be obtained by analogy to the staggered row model, which has already been treated.

Just as in the staggered row model, for the centered honeycomb model there are three spins per unit cell in the Hamiltonian. For each of the solutions with three spins per unit cell, one can map from the staggered row model to the centered honeycomb model. For the staggered row model, each A spin has one η bond and two ordinary bonds to the B spins, and for the centered honeycomb model, each A spin has three η bonds to the B spins. Hence, on replacing $(1+2\eta)$ by 3η, one can go from the three-spins-per-cell solutions for the staggered row model, to the solutions for the centered honeycomb model. In terms of the phase diagram, this means a simple rescaling of the vertical axis in Fig. 3, yielding Fig. 5. The centered honeycomb model, unlike the staggered row model, does not have a preferred direction, and does not

have a preferred wave vector and the complications associated with spiral phases. (Note that we have performed both a $T=0$ analysis and a finite-temperature fluctuation analysis, in search of lower-energy solutions with more than three spins per unit cell. None were found.)

To be specific, scaling from the results of Ref. 21 for the three-spins-per-cell solutions of the staggered row model gives that, for the centered honeycomb model, the AF3-P line is given by $T_c/J=(3/2)\eta$, the NC3-AF3 line is given by $T_c/J=(3/2\eta)$, and the FI-P line is given by $T_c/J=(3/4)(\sqrt{\eta^2+8}-\eta)$. The NC3-FI line is obtained by numerical methods. First, one solves for x in $2\eta=R(6x)/R(3\eta x)$. Then one employs $T_c/J=(3\eta)R(3\eta x)/x$. Note that, for $\eta\rightarrow 1/2$, $x\rightarrow\infty$, and so $T_c/J\rightarrow 0$ for $\eta\rightarrow 1/2$.

As mentioned earlier, Ref. 19 is consistent with either the NC3 or the AF3 phase. On the basis of the mean-field phase diagram, Fig. 5, this argues for a value $\eta>1$. In that case, there should be two phase transitions. Only one seems to be observed. If the signature of the lower transition is subtle (which may well be the case here, since it is not associated with the development of an obvious order parameter, such as the magnetization), it might have been missed. (Although mean-field theory is not by any means exact, it is likely to be qualitatively correct, as long as the system is thermodynamically stable.) On the other hand, the real system is likely to be more complex than the simple model that we have discussed, and so the present discussion may have only limited applicability.

VII. SUMMARY AND CONCLUSIONS

Three generalizations of the fully frustrated triangular lattice of XY spins have been studied: the row model, the staggered row model, and the centered honeycomb model. The staggered row model, with five ordered phases and two tetracritical points, was found to be by far the most complex of the three and has aspects of both of the other two. This may be attributed to the fact that, like the row model, it has a preferred direction and, like the centered honeycomb model, it has three spins per unit cell. Besides the usual mean-field analysis, a phase-fluctuation analysis was performed. In particular, the latter helped provide insight into the nature of the tetracritical points and their relationship to the ground-state solutions. Although a Monte Carlo study indicated that the original analysis (assuming commensurate solutions with three spins per unit cell) was oversimplified and led to the more complete mean-field and fluctuation analyses, a full Monte Carlo study of the staggered row model, including incommensurate boundary conditions, has not yet been performed.

To answer one of the questions that motivated our original considerations, of the three models we have studied the centered honeycomb model, with three spins per unit cell, seems to be most closely analogous, for the FFTR model, to the generalization of Berge *et al.* of Villain's "odd" model of fully frustrated XY spins on the square lattice. Moreover, this model is the most relevant from an experimental viewpoint. This is because the order within the planes of the system $RbFeBr_3$ seems to be described by this model.[17,19] Since the mean-field phase diagram (Fig, 5) indicates that for $\eta>1$, on cooling, the collinear AF3 phase will be attained first, it suggests that, on further cooling, the spins within each plane of $RbFeBr_3$ may undergo a phase transition to the canted NC3 state. It would be of interest to see if such a transition to a canted state does indeed occur.

[1] L. P. Regnault and J. Rossat-Mignod, in *Magnetic Properties of Layered Transition Metal Compounds,* edited by L. J. De Jongh (Kluwer, Dordrecht, Netherlands, 1990), pp. 271–321.

[2] J. Villain, J. Phys. C **10**, 1717 (1977).

[3] H. T. Diep, A. Ghazali, and P. Lallemand, J. Phys. C **18**, 5881 (1985).

[4] B. Berge, H. T. Diep, A. Ghazali, and P. Lallemand, Phys. Rev. B **34**, 3177 (1986).

[5] M. Gabay, T. Garel, G. Parker, and W. M. Saslow, Phys. Rev. B **40**, 264 (1989).

[6] D. H. Lee, J. D. Joannopoulos, J. W. Negele, and D. P. Landau, Phys. Rev. Lett. **52**, 433 (1984).

[7] D. H. Lee, J. D. Joannopoulos, J. W. Negele, and D. P. Landau, Phys. Rev. B **33**, 450 (1986).

[8] D. H. Lee, R. G. Caflisch, J. D. Joannopoulos, and F. Y. Wu, Phys. Rev. B **29**, 2680 (1984).

[9] H. Kawamura, J. Phys. Soc. Jpn. **53**, 2452 (1984).

[10] E. Rastelli, A. Tassi, A. Pimpinelli, and S. Sedazzari, Phys. Rev. B **45**, 7936 (1992).

[11] E. Rastelli, C. Gallenti, S. Sedazzari, and A. Tassi, J. Appl. Phys. (to be published).

[12] T. E. Mason, B. D. Gaulin, and M. F. Collins, Phys. Rev. B **39**, 586 (1989).

[13] C. J. Glinka, V. J. Minkiewicz, D. E. Cox, and C. P. Khattak, in *Magnetism and Magnetic Materials—1973 (Boston),* Proceedings of the 19th Annual Conference on Magnetism and Magnetic Materials, edited by C. D. Graham and J. J. Rhyne, AIP Conf. Proc. No. 18 (AIP, New York, 1974), p. 659.

[14] H. Kawamura, J. Phys. Soc. Jpn. **61**, 1299 (1992).

[15] H. Kawamura, J. Phys. Soc. Jpn. **60**, 1839 (1991).

[16] P. Azaria, B. Delamotte, and T. Jolicoeur, Phys. Rev. Lett. **64**, 3175 (1990).

[17] H. Kawamura, Prog. Theor. Phys. Jpn. Suppl. **101**, 545 (1990).

[18] W. M. Zhang, W. M. Saslow, and M. Gabay, Phys. Rev. B **44**, 5129 (1991).

[19] M. Eibshütz, G. R. Davidson, and D. E. Cox, in *Magnetism and Magnetic Materials—1973 (Boston)* (Ref. 13), p. 386.

[20] A. Harrison and D. Visser, J. Phys. Condens. Matter. **1**, 733 (1990).

[21] G. Parker, W. M. Saslow, and M. Gabay, Phys. Rev. B **43**, 11285 (1991).

[22] W. M. Saslow, M. Gabay and W. M. Zhang, Phys. Rev. Lett. **68**, 3627 (1992).

[23] W. M. Saslow (unpublished).

[24] J. Villain, J. Phys. C **10**, 4793 (1977); **11**, 745 (1978).

[25] T. Kaplan, Phys. Rev. **116**, 888 (1959).

[26] D. H. Lyons and T. Kaplan, Phys. Rev. **120**, 1580 (1960).

[27] T. Kaplan, Phys. Rev. **124**, 329 (1961).

[28] S. Katsura, T. Ido, and T. Morita, J. Stat. Phys. **42**, 381 (1986).

[29] M. Y. Choi and S. Doniach, Phys. Rev. B **31**, 4516 (1985).